JOURNAL OF PROPULSION AND POWER
Vol. 14, No. 1, January–February 1998

Influence of Inlet Pressure Distortion on a Convertible Engine Fan

Tarik Kaya*
International Space University, Strasbourg 67400, France

An experimental and computational study of the flowfield of a fan with uniform and distorted inlet flow is presented. The research facility is a full-scale integrated engine with a constant-speed turbofan. The blade-incidence angles of the fan–rotor can be changed during the operation. Thrust variation is thus achieved by altering the incidence of the fan–rotor blades in the same manner as a variable-pitch propeller. The flowfield of the fan with a uniform inlet flow was first studied by a quasi-three-dimensional approach based on a radial-equilibrium method. The radial-equilibrium solutions are within 1.5–10% of experimental measurements. The results indicated the stable operating range of the fan as a function of the rotor-blade-incidence angles. Then, the results obtained with the uniform inlet flow were used as a reference basis for the study of the distorted inlet flow. The small-perturbation method was very useful to design the distortion screens and to study the propagation characteristic of the distortion. The results revealed that the fan attenuation capacity is augmented when the fan load increases. The distribution of the periodic and random velocity fluctuations at the rotor inlet and outlet was obtained by hot-film probes by using an ensemble-averaging technique. This technique proved to be a useful tool for the assessment of distorted flow characteristics.

Nomenclature

b	=	stream surface thickness
c	=	chord length
F_x	=	axial body force
$DC(60)$	=	circumferential distortion index
I	=	rothalpy
M	=	Mach number
m	=	meridional coordinate
P	=	static pressure
P_t	=	total pressure
R	=	rotor tip radius
R_m	=	radius of curvature
r	=	radial coordinate
t	=	time
v	=	velocity
β	=	angle of relative velocity with the axial direction
γ	=	ratio of specific heats
δP_t	=	normalized total-pressure distortion
ρ	=	density
ϕ	=	streamline slope
ω	=	angular velocity

Subscripts

m	=	meridional direction
r	=	radial direction
x	=	axial direction
θ	=	circumferential direction

Superscripts

$-$	=	mean value
$'$	=	perturbation value

I. Introduction

INLET distortion is generally identified by nonuniform pressure, velocity, and flow angle variations at the engine inlet. A better understanding of inlet distortion-related problems is crucial to achieving successfully integrated next-generation engines. The most significant sources of inlet distortions come from changes in aircraft attitude or shock-wave/boundary-layer interaction causing flow separation in the air intake, wakes from the airframe or other aircraft, ground vortices, crosswinds, and atmospheric turbulence. The distorted inlet flow causes a performance penalty, and may trigger engine instabilities with severe destructive consequences on the engine. Because of its importance, a great deal of study has been devoted to inlet distortion. Comprehensive surveys of previous studies on inlet distortion are summarized in Refs. 1–4.

This study focuses on describing the response of a fan with a variable-incidence rotor to induced total-pressure inlet distortion. In earlier studies, distortion research was based on the rig tests of individual engine components. Reid[5] stated that data obtained by testing isolated components may be very difficult to interpret to make quantitative predictions of the engine tolerance to the distorted-flow conditions. Reid[4] also noted that response and attenuation characteristics of a compressor might be significantly different if tested individually on a test rig. Therefore, the full-scale integrated engine, representing the real operational environment of the fan, was tested for a proper assessment of the fan response to distortion.

The test engine used in this study was designed for application in a unique concept for powering vertical take-off and landing (VTOL) aircraft. This concept involves a convertible engine that can either provide shaft power for turning a lift rotor, or thrust power for horizontal flight. One way of achieving this is to change the blade-incidence angles of the fan–rotor during engine operation. The engine can thus deliver the combination of shaft power and thrust, depending on the rotor-blade-incidence angle. When the blade-incidence angle is in the closed position allowing less mass flow, maximum shaft power can be extracted. With the blades in the open position, maximum thrust is obtained. In the intermediate positions, a combination of shaft power and thrust is possible. Thrust variation is achieved by altering the rotor-blade-incidence angle in the same manner as a variable pitch propeller. The fan geometry is thus variable, and is dictated by the position of the rotor blades. Changing the rotor blade angle significantly modifies blade loading, blade losses, boundary-layer growth, and

Received Jan. 23, 1997; revision received Aug. 4, 1997; accepted for publication Aug. 6, 1997.

*Assistant Professor, School of Engineering, Systems and Technologies. E-mail: kaya@isu.isunet.edu.

blade-row interactions. This leads to different fan pressure ratios for different rotor-blade-incidence angles. The rotor–blade design is obviously one of the main challenges of this concept, because the engine should be operational for a wide range of blade-incidence angles. In this respect, the study of the flowfield through the fan is already quite involved, and the distorted inlet flow conditions introduce an additional complexity.

The VTOL engines using straight-lift or vectored-thrust mode operate in distortion levels approximately three times higher than those encountered by conventional engines.[5] Therefore, they require higher tolerance margins to the inlet distortions. The results obtained in this study suggest that the convertible engine approach for VTOL applications may offer a potential solution to reduce tolerance margins to the inlet distortions. In addition, in comparison to the rotor-driven VTOL applications, the convertible engine makes faster and more efficient horizontal flight feasible, as a result of the available thrust power.

II. Experimental Facility and Instrumentation

The experiments and computations were performed on the Turbomeca-designed Astafan engine. This engine is a single-spool, constant-speed, bypass turbofan with a variable-incidence rotor. The blade-incidence angle can be varied from −8.5 to 35 deg, the 0-deg-incidence angle representing the design condition and the −8.5-deg-incidence angle for the maximum load. The fan design employs 11 rotor blades and 13 stator blades. The design-point overall pressure ratio for the fan stage is 1.25 at a mass flow rate of 34.5 kg/s. The hub-to-tip radius ratio is 0.45 with a rotor tip diameter of 0.558 m. Rotor speed is about 9700 rpm.

The principal instruments used for steady-state measurements were three- and five-hole probes, and thermocouples. The pressure probes were designed to measure the flow angle, and the total and static pressures. These probes were used in combination with pressure transducers, and the output from the transducers was fed into a data processing system to obtain the desired quantities. The errors were estimated at less than 1% in measuring total pressures, and 3–5% in measuring static pressures as a function of Mach number. The error in measuring the yaw and pitch angles of the probes was ±1 deg. The traversing mechanisms used had two degrees of freedom: 1) linear motion along the radial direction of the fan and 2) rotation of the probe around its own axis. An additional error of ±0.5 deg was estimated in the alignment of the probes along the fan axis.

For unsteady measurements, X hot-film probes were calibrated as a function of the flow speed and angle. The error in the measurement of the random and periodic velocity fluctuations was less than 2%.

All measurements were taken with a computerized data acquisition system. The data were first stored and then analyzed. Details of the instrumentation and the measuring methods developed are discussed in Ref. 6.

III. Uniform Inlet Flow

A detailed study of the fan flowfield was first performed with uniform inlet flow. The results of this study served as a reference base for the study of the engine performance characteristics with inlet distortion. The numerical method used combines the radial-equilibrium and the blade-to-blade solutions for a quasi-three-dimensional representation of the fan flowfield.[7] The radial-equilibrium solutions were compared with the results of the steady-state measurements. The results were obtained for different blade-incidence angles to identify the on- and off-design operating conditions.

A. Radial-Equilibrium Solution

The flow through the fan was assumed to be axisymmetric between the blade rows. The governing equations of a steady, inviscid, compressible, adiabatic flow of a perfect gas with constant specific heats in the absence of the external body forces were considered. The radial-equilibrium equation in terms of the Mach number can be given by the following equation:

$$\left(1 - \frac{M_x^2}{\cos^2\phi}\right)\frac{1}{\gamma P}\left(\frac{\partial P}{\partial r}\right) = (1 - M_x^2)\frac{M_\theta^2}{r} + M_x^2\frac{tg^2\phi}{r} + M_x^2\frac{tg\phi}{\cos^2\phi}\frac{\partial\phi}{\partial r} - \frac{M_x^2(1 - M_x^2)}{R_m\cos^3\phi} \tag{1}$$

where

$$M_x = M\cos\phi\cos\beta \tag{2a}$$

$$M_\theta = M\sin\beta \tag{2b}$$

$$M_m = M\cos\beta \tag{2c}$$

Equation (1) was solved by using a fourth-order Runge–Kutta scheme. The calculations were performed at the inlet and outlet of the rotor. The solution method required an iterative procedure. The mass conservation equation was used to check the convergence of iterations. The deviation angles and the relative flow losses were taken into account by means of correlations, which are described in detail in Ref. 8.

B. Results

The steady-state measurements were carried out at 11 radial locations at the inlet and the outlet of the rotor for a set of rotor-blade-incidence angles. The measurement locations are shown in Fig. 1. The radial-equilibrium calculations were obtained at the same planes where the measurements were taken. Figures 2 and 3 show the comparison between these measurements and the numerical solutions for the blade-incidence angles of −5 and +5 deg. The radial distributions of normalized static pressure and the relative flow angle at the inlet and outlet are represented in Figs. 2 and 3. The results of static-pressure calculations are within 0.6–4.5% of the experimental measurements. The comparison of the static-pressure measurements and the calculations is more satisfactory in the midregion where the radial gradients are negligible. As shown in Figs. 2b and 3b, the static-pressure distribution near the tip region at the outlet was not well predicted (within 4.5%). This is because of the secondary flow and clearance flow effects near the tip. The numerical method used in this study cannot simulate these effects. The relative flow angles were predicted within 1.5–10% of the experimental measurements. The flow angles near the tip at the outlet were not well predicted because of the same reasons. The negative inlet flow angle is clear in Fig. 3c for the +5-deg-blade-incidence angle. The difference between the numerical values and the measurements near the hub (about 10%) in Fig. 3d could be explained by a possible flow separation caused by these negative inlet flow angles. The results obtained for higher values of the incidences showed that the inlet flow angles become more negative, and the fan

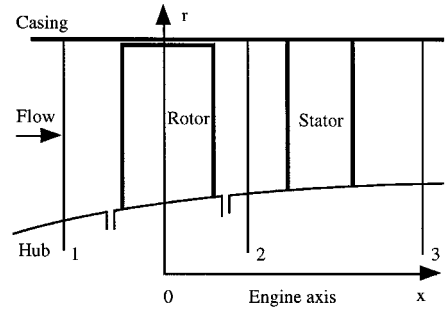

Fig. 1 Fan test section showing measurement planes. (x_1/R = 0.34, x_2/R = 0.28, x_3/R = 0.88, where R = 0.279 m.)

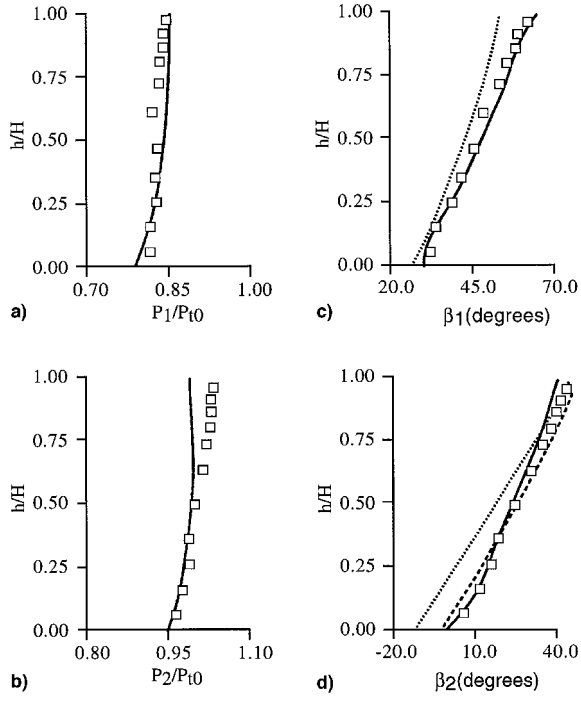

Fig. 2 Comparison of measurements and calculations for the −5-deg-blade-incidence angle: a) normalized static pressure at the inlet, b) normalized static pressure at the outlet, c) relative flow angle at the inlet, and d) relative flow angle at the outlet. ——, radial-equilibrium calculations; ----, flow deviation correlations; · · · · ·, solid blade angles; □, experimental results.

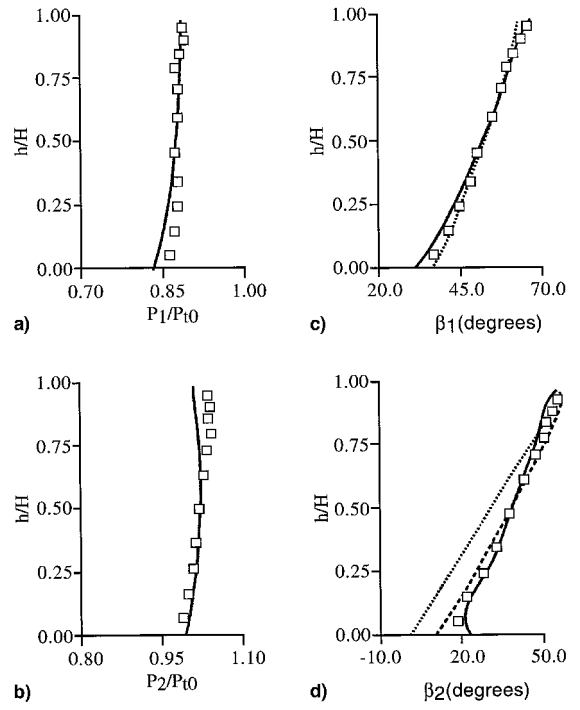

Fig. 3 Comparison of measurements and calculations for the +5-deg-blade-incidence angle: a) normalized static pressure at the inlet, b) normalized static pressure at the outlet, c) relative flow angle at the inlet, and d) relative flow angle at the outlet. ——, radial-equilibrium calculations; ----, flow deviation correlations; · · · · ·, solid blade angles; □, experimental results.

is in the far off-design operating regime. The deviation angles were also calculated separately by using empirical correlations. The results of these correlations are within 10% agreement of the experimental measurements (Figs. 2d and 3d). The deviation angle correlations were also valid for the off-design conditions.

C. Blade-to-Blade Solution

A blade-to-blade solution was performed to complete the quasi-three-dimensional analysis of the rotor with a uniform inlet flow. The unsteady Euler equations were integrated by a finite difference scheme of the predictor–corrector type using MacCormack's method[9] to obtain the steady-state solutions. Because the solutions of interest here were only the final steady-state solutions, the equation of energy was replaced by its simple steady form to reduce the required computer time and memory.[10] The governing equations in the curvilinear coordinates (m, θ, and x) may be written as

$$\frac{\partial}{\partial t}(br\rho) + \frac{\partial}{\partial m}(br\rho v_m) + \frac{\partial}{\partial \theta}(b\rho v_\theta) = 0 \tag{3}$$

$$\frac{\partial}{\partial t}(br\rho v_m) + \frac{\partial}{\partial m}[br(P + \rho v_m^2)] + \frac{\partial}{\partial \theta}(b\rho v_m v_\theta) = P\frac{\mathrm{d}}{\mathrm{d}m}(br) + b\rho(v_\theta + \omega r^2)\frac{\mathrm{d}r}{\mathrm{d}m} \tag{4}$$

$$\frac{\partial}{\partial t}(br\rho v_\theta) + \frac{\partial}{\partial m}(br\rho v_m v_\theta) + \frac{\partial}{\partial \theta}[br(P + \rho v_\theta^2)] = -b\rho v_m(v_\theta + 2\omega r)\frac{\mathrm{d}r}{\mathrm{d}m} \tag{5}$$

$$\frac{\partial}{\partial t}[br(\rho I - P)] + \frac{\partial}{\partial m}(br\rho v_m I) + \frac{\partial}{\partial \theta}(b\rho v_\theta I) = 0 \tag{6}$$

The radial-equilibrium solutions provide the necessary information to calculate the shape of the streamlines in the meridional plane. The stream surfaces were then assumed to be the surfaces of revolution. The intersection of a chosen stream surface with the three-dimensional blade geometry provided the solution domain between the two successive blades.

The viscous effects were introduced by using semiempirical relations.[11] All of the results were obtained by implementing a nonreflecting downstream boundary condition. This condition permits the cutoff of information from downstream and brings downstream infinity at a finite distance. Convergence was assumed to occur when the pseudotime derivatives of the velocity components were smaller than 10^{-4}. The converged results were used to refine the results of the radial-equilibrium solutions, and this cycle between the radial-equilibrium and the blade-to-blade solutions was repeated until the stream surface coordinates did not change more than 0.3% at all grid points over approximately 10 iterations. More information on the calculation procedure and boundary conditions can be found in Refs. 6 and 11.

D. Results

Results are provided in Figs. 4, 5, and 6 for the blade-incidence angles of 0, −5, and +5 deg, respectively, at the tip (90% of the blade height), mid (50%), and hub (10%) sections. In Fig. 4, the Mach number contours for the 0-deg-incidence angle show only a small low-supersonic region at the blade tip. Also shown in Fig. 4 is the pressure distribution for the hub showing that the flow was rapidly compressed and expanded in the neighborhood of the leading and trailing edge on the upper surface of the blade. This is a result of the coarse mesh used to represent these regions. To minimize the computational time and memory, the mesh size was optimized by a series of test runs. The flowfield was first calculated by using a very fine mesh. Then, mesh size was increased until the maximum percentage change of the stream surface values at the corresponding points in the whole solution domain was

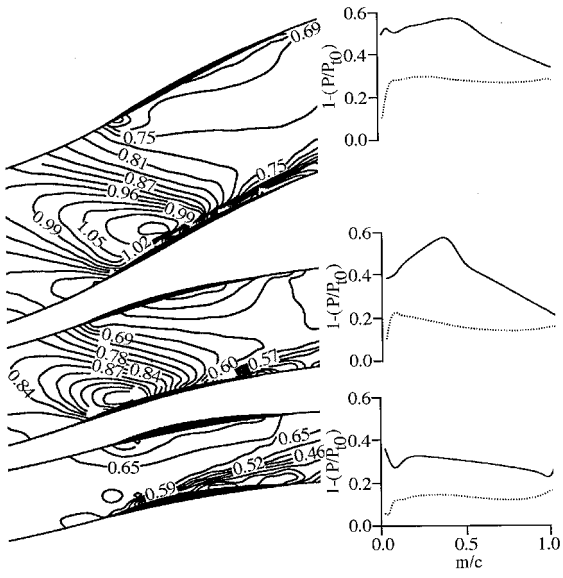

Fig. 4 Mach number contours for the 0-deg-blade-incidence angle, from top to bottom, at the tip (90% of the blade height), mid (50%), and hub (10%) sections with the corresponding static-pressure distributions on the blade. ——, upper blade surface; · · · · ·, lower blade surface.

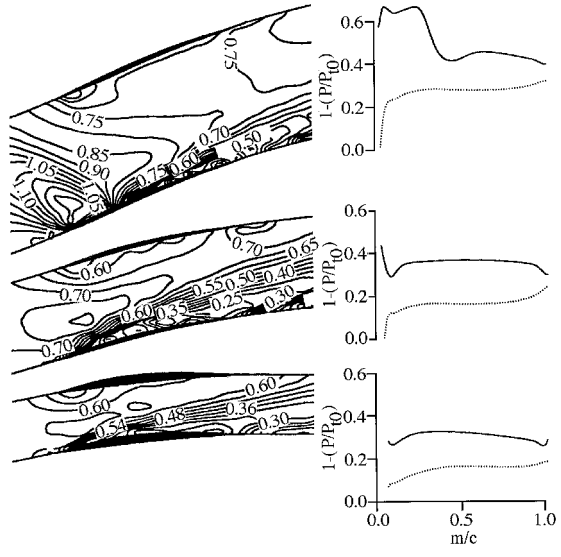

Fig. 5 Mach number contours for the −5-deg-blade-incience angle, from top to bottom, at the tip (90% of the blade height), mid (50%), and hub (10%) sections with the corresponding static-pressure distributions on the blade. ——, upper blade surface; · · · · ·, lower blade surface.

less than 0.5%. The influence of the coarse mesh was more noticeable in the hub section of the profile, which is thicker than the other two sections represented.

Figure 5 shows the results for the −5-deg-incidence angle, which is close to the maximum flow design condition of the blade incidence (−8.5 deg). A weak shock was predicted on the upper surface at the tip section. The corresponding compression as a result of this shock is clear on the static-pressure distribution in Fig. 5.

In Fig. 6, for the +5-deg-blade-incidence angle, the negative inlet flow angles are evident on the static-pressure distribution plots for three sections: hub, mid, and tip. A rear shock on the upper surface of the blades at the hub and tip sections was located as a result of off-design operation. No convergence was obtained for the higher blade-incidence angles. For these angles, the three-dimensional and viscous flow effects become

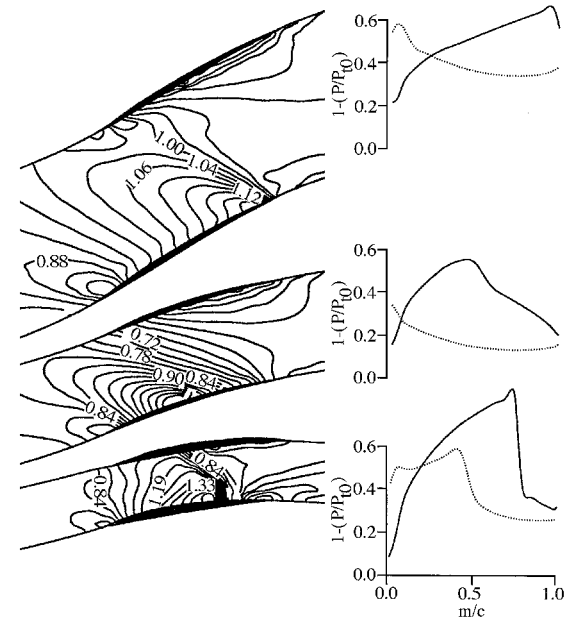

Fig. 6 Mach number contours for the +5-deg-blade-incidence angle, from top to bottom, at the tip (90% of the blade height), mid (50%), and hub (10%) sections with the corresponding static-pressure distributions on the blade. ——, upper blade surface; · · · · ·, lower blade surface.

more dominant, and these flow characteristics were not captured by the quasi-three-dimensional method.

IV. Nonuniform Inlet Flow

This section focuses on the effects of an induced total-pressure distortion on the fan performance. The computational and experimental study of the fan flowfield with a uniform inlet flow allowed a better understanding of the fan design conditions as functions of the rotor-blade-incidence angles. In this part of the paper, a small-perturbation analysis is first described to study the propagation characteristics of distortion through the fan and the distortion attenuation capacity of the fan. Unsteady measurements obtained by X hot-film probes are then discussed.

A. Small-Perturbation Analysis

The inlet pressure distortion was simulated by using gauze screens. A rapid and simple method was required to design these distortion screens and to determine the optimum distance between the distortion screen and the fan. The distortion screen should be placed far enough from the engine to allow the flow redistribution of the perturbed flow. However, if the distortion screen is placed too far from the engine, the generated distortion might be significantly attenuated before arriving at the fan. In addition, the distortion leaving the fan may influence the other components of the engine downstream. The amplitude of the generated distortion should then be small enough not to cause a significant loss of the engine surge margin for a safe operation. The linearized theory was a good approach to quickly calculate the flow redistribution upstream and the propagation of the distortion pattern throughout the fan as a function of the rotor-blade-incidence angle.

The method used in this work was based on the linearized theory developed by Plourde and Stenning.[12] This method is applicable to the small-amplitude circumferential distortions of the total pressure. In this model, an inviscid, incompressible, steady two-dimensional flow was considered, and the pressure rise characteristics of the fan were simulated by the equivalent body forces. The flow variables were first expressed under the form of the sum of a mean flow and small perturbations:

$$\nu = \bar{\nu} + \nu' \qquad (\nu' << \bar{\nu}) \tag{7}$$

The Euler and continuity equations were then linearized by using the approach in Eq. (7). The resulting Euler equations in axial and circumferential directions were cross-differentiated and subtracted from one another to eliminate the explicit appearance of the pressure. The resulting equations are as follows:

$$\frac{\partial^2 v_x'}{\partial x \partial \theta} - r\frac{\partial^2 v_\theta'}{\partial x^2} = \frac{1}{\rho \bar{v}_x}\frac{\partial F_x'}{\partial \theta} \tag{8}$$

$$\frac{1}{r}\frac{\partial v_\theta'}{\partial \theta} + \frac{\partial v_x'}{\partial x} = 0 \tag{9}$$

The linear character of the resulting equations allows a Fourier series solution. The resistance to flow in the tangential direction was introduced by an empirical parameter, which is a function of the solidity of the blading and the clearance between the blade rows. As stated by Plourde and Stenning,[12] it is found that although the velocity distribution is influenced by this empirical parameter, the overall attenuation is almost constant over the range of possible values varying from 1 (very large axial clearances) to ∞ (zero axial clearances). Plourde and Stenning[12] also showed that the approximation of no cross-flow within the compressor gives excellent results.

B. Results

The inlet total-pressure distortion was generated by a gauze screen with a spoiled sector angle of 30 deg. A fixed rake probe array with 10 equispaced rakes and five total-pressure probes per rake was used to measure the distortion patterns. The rake was placed at one radius upstream of the engine face. The resulting total-pressure distortion was represented by the Fourier series expansion, which provided the input values for the small-perturbation analysis.

An important parameter of the linearized theory was the slope of the corrected constant speed of the fan on the compressor characteristic map (nondimensional mass flow vs pressure rise) for a given rotor-blade-incidence angle. Because the test engine was a constant-speed turbofan, the equation for the corrected speed was determined by using five exit nozzles of different geometrics for each rotor-blade-incidence angle. Reid[5] stated that the compressor nondimensional performance, i.e., nondimensional mass flow and efficiency, is only slightly affected by distortion, particularly by predominantly circumferential distortions, and that the variations are generally within $\pm 2\%$ of the undisturbed values. Thus, because of the nature of the distortion considered in this work (primarily circumferential with a spoiled sector angle of only 30 deg), the equation for the corrected speed obtained with uniform inlet flow was used in the estimation of the distorted flow characteristics.

Figures 7 and 8 show, respectively, the evolution of the circumferential total-pressure distortion at the midsection through the fan for the incidence angles of -5 and $+5$ deg. The total-pressure values δP_t represented here are the sum of the amplitude of the generated total-pressure distortion and the perturbation introduced by the fan on the upstream flowfield. All of the values were normalized by the mean total pressure. The fan extends from $x/R = 0$ to 0.931, where x is the axial distance and R is the fan tip radius. In Figs. 7 and 8, the valley of low-pressure region is induced by the distortion screen. The other two low-pressure regions on the right and left of this valley are a result of the braces of the backup screen, which serves as a support to the distortion screen.

The distortion at the inlet for the -5-deg-incidence angle is 8% stronger than that for $+5$ deg, based on $DC(60)$. This is because the fan is highly loaded for the -5-deg-incidence angle, and the inlet velocities are therefore higher. The total-pressure losses increase when the flow with higher velocity passes through the distortion screen. To quantify the overall attenuation capacity of the fan, the recovery ratio [RR = 1 $-$ $(\delta P_{t2}/\delta P_{t1})$] introduced by Smith,[13] was used. The fan overall recovery ratio for -5-deg-incidence angle was 7% higher than that for the $+5$-deg-incidence angle. Because the fan is highly loaded for -5-deg-incidence angle, it can furnish more work to the region of deficient energy, which in turn, improves the fan attenuation capacity. This would be consistent with Longley and Greitzer's[1] statement that, the steeper the compressor characteristics, the greater the distortion attenuation. Longley and Greitzer[1] also noted that because the greater pressure rise in the low-flow region implies a greater work input, a higher total temperature distortion would be induced downstream of the compressor.

In Fig. 9, the δP_t values are plotted against the axial distance for -5- and $+5$-deg-blade-incidence angles. The calculated δP_t values are seen to be 5–15% higher than those derived from experimental measurements. Because neither unsteady flow dynamics nor nonlinear effects is taken into account, the

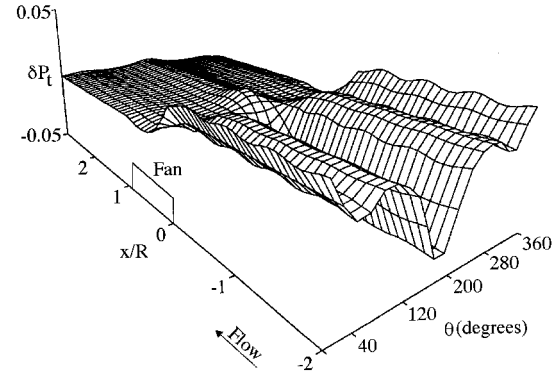

Fig. 7 Evolution of the circumferential total-pressure distortion at the midsection (50% of the blade height) through the fan for the −5-deg-blade-incidence angle.

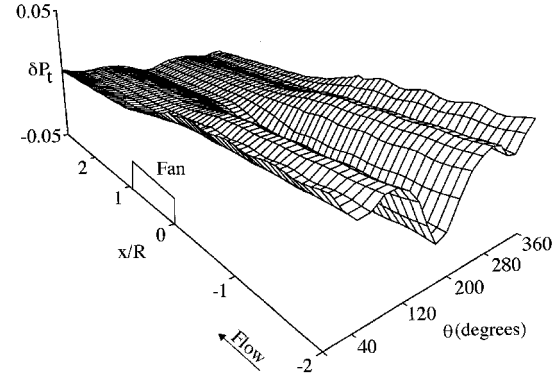

Fig. 8 Evolution of the circumferential total-pressure distortion at the midsection (50% of the blade height) through the fan for the +5-deg-blade-incidence angle.

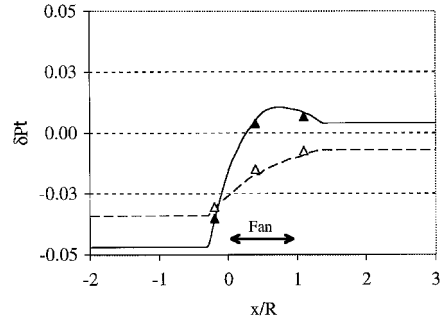

Fig. 9 Comparison of experimental and theoretical results. ——, theory; ▲, measurements for −5-deg-blade-incidence angle; and ----, theory; △, measurements for +5-deg-blade-incidence angle.

small-perturbation theory cannot be used for an accurate estimate of the loss of stability margin.[14] However, as shown in Fig. 9, because the model underestimates the fan attenuation capacity, the stability assessment by using the small-perturbation theory would be on the conservative side. The simple parallel compressor model also always overestimates the loss of stability margin.[15] Note that the distortions of the small circumferential extent have little effect on stability.[1] As a result, it would be reasonable to use the small-perturbation theory for a fair estimation of the safe operating range of the fan. It was important to ensure that the gas-generator or the hub section was not operating on the stalled side of the fan characteristics. In the case of a hub section surge, the distortion leaving the hub section would be significantly amplified, which may be the source of trouble for the following compressor and other components. We used the criterion suggested by Stenning[16] to analyze the fan stability. According to this criterion, the infinite amplification of any inlet distortion is associated with the occurrence of a rotating stall. By using this approach, we estimated that the engine would be within the limits of stable operation if the distortion screens were placed at the position of 1.4 fan diameters upstream. This distance allows a safe operating range for the introduced distortion and also an optimized flow redistribution upstream of the fan.

C. Unsteady Measurements

The measurements were taken by using X hot-film probes and a distortion screen with a spoiled sector angle of 30 deg. Hot-film probes were placed at both the inlet and outlet of the fan rotor. The data obtained from the probes were sampled at 2048 points over 45 revolutions of the rotor. The sampling frequency was selected at 100 kHz. The A/D converter has a 12-bit resolution at an input range of ±10 V. The measurements were triggered by an optical sensor that can detect the passage of a black-painted blade tip with an accuracy of ±1/10 rpm. The distortion screen was also rotated to take into account the influence of the screen location with respect to the hot-film position. The data represented here correspond to the results obtained from the hot-film probes located within the perturbed flow region by the distortion screen. The axial and tangential components of the flow velocity in the duct were simultaneously measured with the X hot-film probes. Note that outside the areas close to the hub and the casing, the radial velocities are negligible, and the use of X hot-film probes to obtain the resultant flow velocity is appropriate.

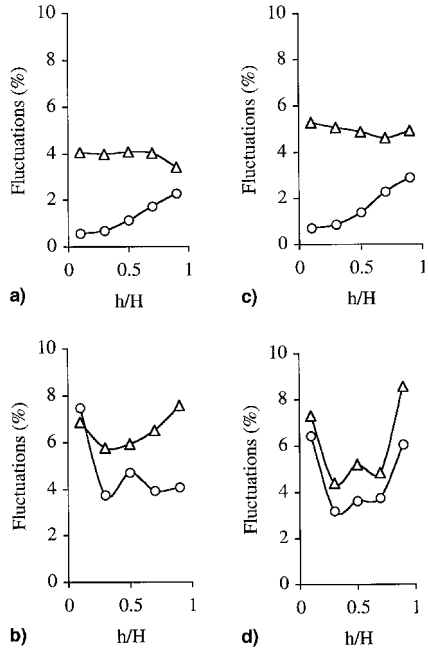

Fig. 10 Random and periodic velocity fluctuations normalized by the time-averaged mean value of the absolute velocity for the −5-deg-blade-incidence angle: a) at the rotor inlet with uniform inlet flow, b) at the rotor outlet with uniform inlet flow, c) at the rotor inlet with distorted inlet flow, and d) at the rotor outlet with distorted inlet flow. △, random fluctuations; ○, periodic fluctuations.

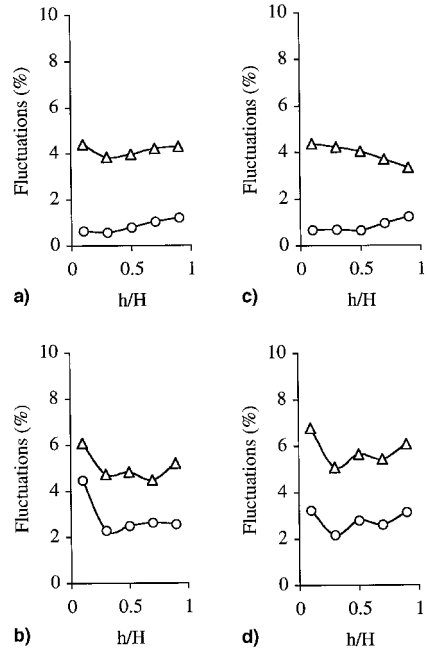

Fig. 11 Random and periodic velocity fluctuations normalized by the time-averaged mean value of the absolute velocity for the +5-deg-blade-incidence angle: a) at the rotor inlet with uniform inlet flow, b) at the rotor outlet with uniform inlet flow, c) at the rotor inlet with distorted inlet flow, and d) at the rotor outlet with distorted inlet flow. △, random fluctuations; ○, periodic fluctuations.

By using an ensemble-averaging technique, the periodic and random velocity fluctuations were separated. The details of this technique are discussed in Refs. 17 and 18. The estimation of the maximum error of the measurements results in 2% accuracy with a probability of 0.9.[19]

The periodic and random fluctuation profiles at the inlet and outlet of the rotor for the −5- and +5-deg-blade-incidence angle are plotted in Figs. 10 and 11, respectively. All of the values were normalized by the time-averaged mean value of the absolute velocity. The measurements were taken at the five different radial locations of 10, 30, 50, 70, and 90% of the blade height. The results obtained in the absence of a distortion screen are also presented for comparison. The distortion backup screen was maintained during all of the tests to have a reference base. The level of random fluctuations measured without the distortion screen at the inlet was approximately 1.3 times higher than expected because of this backup screen.

As shown, respectively, in Figs. 10a and 10c for −5 deg, and in Figs. 11a and 11c for +5 deg, the form of the periodic fluctuations measured at the inlet with and without inlet distortion exhibits considerable resemblance, and their levels were slightly increased in the case of distorted inlet flow (less than 1.2 times). This evenly distributed augmentation of the periodic fluctuations at the inlet appears to be related to the flow redistribution effects induced by the fan–rotor at the fan upstream. Because our test engine is at a constant speed, the blade-induced frequencies are constant in both cases, with and without inlet distortion. However, the level and form of the random fluctuations were noticeably influenced by the distortion, as shown in Figs. 10a, 10c, 11a, and 11c. This must be a result of the increased level of turbulence originated by the distortion screen with a fine mesh (42% permeability). At the

same time, for the −5-deg-blade-incidence angle, because the inlet velocity is 9% higher than that for +5 deg, the augmentation of the random fluctuations is more pronounced up to 30%, as shown in Figs. 10a and 10c.

At the outlet of the rotor, the augmentation of the random fluctuations in correspondence with increasing losses near the hub and the casing is clear with and without the distortion screen. Binder et al.[18] measured the fluctuations in a multistage low-pressure turbine by using a similar technique. The rising shape of the random fluctuations near the hub and casing is inconsistent with Binder et al.'s[18] results. The radial variation of the fluctuations was clearly amplified (35%) for the −5-deg-blade-incidence angle in the case of distorted flow (Fig. 10d). Note that the periodic fluctuations are decreased at the hub (15–35%) in the case of distorted flow for the whole range of blade-incidence angles tested. This decrease in the periodic fluctuations, accompanied by an increase in random fluctuations at the hub, suggested a possible flow separation near the hub. This would be consistent with the earlier results obtained with uniform inlet flow for +5-deg-blade-incidence angle (see Sec. III.B). This finding also suggests that the inlet distortion would induce a flow separation near the hub for −5 deg. As explained by Reid,[5] during testing fans of bypass engines, there may be difficulty in deciding whether the bypass (tip) or the gas-generator (hub) sections will cause an engine surge. The suggested measurement and evaluation technique may therefore help to identify which section is the source of trouble for the components downstream, and thus to reduce the design risk.

Another remarkable observation is the increase of the random and periodic fluctuation levels (10–30%) in the midspan area caused by distortion. This phenomenon is more pronounced when the fan is highly loaded and the blade incidences are higher than 0 deg. The fluctuation patterns could also be used to analyze the trends of the efficiency distributions in the various stages.[18] Thus, the results also indicate how the introduced distortion causes an efficiency penalty across the span.

As stated earlier, the distortion screen was rotated with respect to the hot-film position to take measurements at four different circumferential positions, each spaced apart from the other by 90 deg. This was to see the effect of the introduced distortion on the unspoiled regions. The fluctuation patterns for these regions exhibit a similar behavior to the results obtained with uniform inlet flow, suggesting no strong impact of the distortion on the unspoiled regions. This is probably attributable to the nature and low extent of the distortion considered in this study. Chue et al.[15] studied the compressor stability by considering a model of the fluid dynamic interaction between the spoiled and unspoiled sectors of the compressor. They showed the importance of interaction between the high and low total-pressure sections for more intense distortions (a spoiled sector of 120 deg). However, they did not consider the distortions of smaller extents, and no comparison was possible between their data and our results.

As a result of all of these observations, it would be reasonable to conclude that the inlet distortion is transferred through the fan–rotor by a complex transfer mechanism. Also note that the frequency analysis of these signals did not reveal any indication of the rotating stall in the case of distorted inlet flow. This result is consistent with the small-perturbation model predictions regarding the occurrence of the rotating stall (see Sec. IV.B, last paragraph).

V. Summary and Conclusions

A comprehensive experimental and numerical survey of the flowfield through a fan with an inlet total-pressure distortion was presented. The test engine used was a convertible type with a fan–rotor having variable-incidence blades. The flowfield through this fan was particularly complex, because blade loading, blade losses, boundary-layer growth, and blade-row interactions were significantly modified when the rotor blade angles were changed.

The study of the fan flowfield with uniform inlet flow provided the reference basis for the case of the distorted inlet flow. The radial-equilibrium solutions are within 1.5–10% of the steady-state measurements. It was shown that the quasi-three-dimensional code and associated loss and flow turning correlations (within 10%) were satisfactory for predicting the undisturbed performance of the fan flow, both for on- and off-design conditions. The quasi-three-dimensional model was used to determine the limits of the design operating regime of the fan. The numerical method was valid to study the fan flowfield for the blade-incidence angles ranging from −8.5 to +5 deg; 0 deg representing the optimum design angle.

The small-perturbation theory was very useful in designing the distortion screens and in optimizing the distance between the distortion screen and the fan. The distortion screens were thus placed 1.4 fan diameters upstream of the fan. The model appears to be in accord with the experimental results, and can be used for a reasonable assessment of the occurrence of the rotating stall in the case of an inlet distortion of small circumferential extent (about 30 deg).

The measurements taken by X hot-film probes were analyzed by using an ensemble-averaging technique. It was shown that this technique could be a very useful tool for the analysis of the distorted inlet flow behavior. At the rotor inlet, the periodic fluctuations with and without inlet distortion show considerable resemblance in shape. At the rotor outlet, the distortion mainly affects the random fluctuations, but affects the periodic fluctuations less. The results suggest a possible flow separation near the hub, which is found to be consistent with the results obtained with uniform inlet flow. No important interaction is found between the spoiled and unspoiled sectors because of the nature and low extent of the distortion considered in this study. The results of measurements of the periodic and random fluctuations suggest a complex transfer of distortion patterns through the fan–rotor. Additional research is required to understand the relation between the transfer of these fluctuations and the onset of distortion-induced instabilities.

The results obtained in this study have also shown that the attenuation capacity of the fan is increased when the fan is more loaded (−8.5-deg-blade-incidence angle corresponds to the maximum load). Thus, the fan can provide more work to the low-energy region created by the distorted sector of the inlet flow, demonstrating the usefulness of using a convertible engine to reduce the tolerance margins to inlet distortion. Because the VTOL engines with straight-lift, vectored-thrust, and highly curved ducts operate in significantly high inlet distortion levels, the convertible engine provides an efficient option to power the VTOL vehicles.

Acknowledgments

This research was conducted at the Propulsion Laboratory of Ecole Nationale Supérieure de l'Aéronautique et de l'Espace (ENSAE), France, and was supported by a French government grant. The help of G. Meauzé, ONERA, Paris; R. Barènes and A. Carrère, ENSAE; and C. Camci, PennState, is greatly appreciated. The author also thanks Turbomeca, France, for providing the test engine and related technical data.

References

[1]Longley, J. P., and Greitzer, E. M., "Inlet Distortion Effects in Aircraft Propulsion System Integration," *Steady and Transient Performance Prediction of Gas Turbine Engines*, AGARD N92-28458, 1992.

[2]Williams, D. D., "Review of Current Knowledge on Engine Response to Distorted Inflow Conditions," *Engine Response to Distorted Inflow Conditions*, CP-400, AGARD, 1987.

[3]Fuhs, A. E., "Introduction to Distortion Induced Engine Stability," *Distortion Induced Engine Instability*, LS-72, AGARD, 1974.

[4]Williams, D. D., and Yost, J. O., "Some Aspects of Inlet/Engine Flow Compatibility," *Aeronautical Journal*, Sept. 1973, pp. 483–492.

[5]Reid, C., ''The Response of Axial Flow Compressors to Intake Flow Distortion,'' American Society of Mechanical Engineers, 69-GT-29, New York, 1969.

[6]Kaya, T., ''Etude Expérimentale et Numérique du Fonctionnement d'une Soufflante à Calage Variable en Présence d'une Distorsion de Pression Totale en Entrée,'' Ph.D. Dissertation, Ecole Nationale Supérieure de l'Aéronautique et de l'Espace, Toulouse, France, Feb. 1993.

[7]Bosman, C., ''Quasi-Three-Dimensional Numerical Solution of Flow in Turbomachines,'' American Society of Mechanical Engineers, 76-FE-23, New York, 1976.

[8]Miton, H., Doumandji, Y., and Chauvin, J., ''Simplified Method for Flow Analysis and Performance Calculation Through an Axial Compressor,'' American Society of Mechanical Engineers, 84-GT-250, New York, 1984.

[9]MacCormack, R. W., ''The Effect of Viscosity in Hypervelocity Impact Cratering,'' AIAA Paper 69-354, May 1969.

[10]Viviand, H., and Veuillot, J. P., ''Méthodes Pseudo-Instationnaires pour le Calcul d'Ecoulements Transsoniques,'' ONERA, No. 580, Paris, April 1978.

[11]Meauzé, G., and Paulon, J., ''Simulation Numérique des Ecoulements non Réactifs dans les Turbomachines,'' *La Recherche Aérospatiale*, No. 2, March/April 1990, pp. 39–58.

[12]Plourde, G. A., and Stenning, A. H., ''The Attenuation of Circumferential Inlet Distortion in Multi-Stage Axial Compressors,'' *Journal of Aircraft*, Vol. 5, No 3, 1967, pp. 236–242.

[13]Smith, L. H., ''Recovery Ratio—a Measure of the Loss Recovery Potential of Compressor Stages,'' *Transactions of American Society of the Mechanical Engineers*, Vol. 80, No. 3, 1958.

[14]Hynes, T. P., and Greitzer, E. M., ''A Method for Assessing Effects of Circumferential Flow Distortion on Compressor Stability,'' *Journal of Turbomachinery*, Vol. 109, July 1987, pp. 371–379.

[15]Chue, R., Greitzer, E. M., Tan, C. S., Hynes, T. P., and Longley, J. P., ''Calculations of Inlet Distortion Induced Compressor Flow Field Instability,'' *International Journal of Heat and Fluid Flow*, Vol. 10, Sept. 1989, pp. 211–223.

[16]Stenning, A. H., ''Inlet Distortion Effects in Axial Compressors,'' *Journal of Fluids Engineering*, Vol. 102, March 1980, pp. 7–13.

[17]Pfeil, H., and Sieber, J., ''Velocity Distribution and Decay Characteristics of Wakes Behind a Compressor Rotor-Blade,'' American Society of Mechanical Engineers, 86-GT-115, New York, 1986.

[18]Binder, A., Schroeder, T., and Hourmouziadis, J., ''Turbulence Measurements in a Multistage Low Pressure Turbine,'' American Society of Mechanical Engineers, 88-GT-79, New York, 1988.

[19]Cousteix, J., *Turbulence et Couches Limites*, Ecole Nationale Supérieure de l'Aéronautique et de l'Espace, Toulouse, France, 1988.